ADVANCED FUNCTIONAL MATERIALS

www.afm-journal.de

Biologization of Allogeneic Bone Grafts with Polyphosphate: A Route to a Biomimetic Periosteum

Werner E. G. Müller, Shunfeng Wang, Maximilian Ackermann, Torsten Gerich, Meik Neufurth, Matthias Wiens, Heinz C. Schröder, and Xiaohong Wang**

The physiological polyphosphate (polyP), released primarily from platelets after bone fractures, acts as a donor for metabolic energy and as a phosphate source for bone mineralization. In this study allogeneic, decellularized bone samples are biologized with a layer of inorganic polyP by submersion of human femur cortex slices into a solution of Na-polyP. Then polyP coat is modified by exposure to $CaCl_2$, resulting in in situ formation of amorphous Ca-polyP microparticles (Ca-polyP-MP; diameter of ≈155 nm). Energy dispersive X-ray spectroscopy analysis of the Ca-polyP-MP coat reveals a Ca:P molar ratio of ≈0.78, while the nonmodified bone cortex is characterized by a Ca:P ratio of ≈1.52. An ionic shift promotes the strong binding of the polyP to the bone. While the polyP modification only insignificantly increases the hardness of the bone sample, without changing the elastic surface properties, the polyP-modified bone provides a very favorable substrate for SaOS-2 cells to attach and to mineralize. In the presence of medium/serum the polyP coat transforms to a functionally active coacervate. The cells, attached to the polyP coat, show a marked spreading behavior and became entrapped into the polyP-coacervate. The results suggest that regenerative-active polyP might be of potential use in healing of bone.

1. Introduction

According to the embryological origin the process of bone formation, osteogenesis or ossification, is classified into two types. First, intramembranous [periosteal] ossification that proceeds within the mesenchymal cell lineage during which these cells differentiate into osteoblasts without preceding cartilage formation and second, endochondral [endosteal] ossification a morphogenetic process of bone mineralization that occurs after cartilage formation (reviewed in ref. [1]). The key structure from where the formation and regeneration of bone, as well as the repair of wounds, during the intramembranous [periosteal] ossification is initiated and maintained is the periosteum. This dense, fibrous membrane overlays the outer surface of all bones with the exception of the joints of long bones.

The periosteum is composed of two layers: the outer "fibrous layer" and the inner "cambium layer."[2] The fibrous layer is further subdivided into the superficial coat which is more rigid and relatively cell poor, and the fibroelastic layer.[3] The collagenous fibers in the superficial portion are arranged in small compact bundles into which elongated fibroblasts are interspersed. This part is the most highly vascularized region within the periosteum and the main blood contributor to bone and skeletal muscle. In addition, this region is highly innervated. The deeper part of the outer fibrous layer is termed fibroelastic layer since it incorporates elastic fibers, providing this layer with highly elastic properties. Additionally it is composed of many collagenous fibers, and it is cell poor and not highly vascularized.

In contrast, the inner cell rich cambium layer of the periosteum is rich in stem cells. Recently it has been disclosed that the stem cells present in this layer, the periosteal stem cells, show transcriptional signatures that make them different from other skeletal stem cells and also from mature mesenchymal cells.[4] In contrast to stem cells that form mineralic bone deposits via initial cartilage template in the endochondral pathway,[5] the periosteal stem cells play crucial roles in both fracture healing and modeling of the bone cortex.

The periosteum is not only involved in bone formation but also in wound repair. This function has been proven by findings that periostin, a protein highly expressed in the periosteum, can bind as a ligand to epithelial-specific integrins affecting migration of epithelial cells.[6]

Focusing on the bone-exposed part of the periosteum the function of this layer is not only restricted to the repair-inducing stem cells, the periosteal stem cells, that induce mineralization, but also most likely to polyphosphate (polyP) that is involved in the supply of phosphate and metabolic energy for the growing bone. As

Prof. W. E. G. Müller, Dr. S. Wang, Dr. M. Neufurth, Dr. M. Wiens, Prof. H. C. Schröder, Prof. X. H. Wang
ERC Advanced Investigator Grant Research Group at the Institute for Physiological Chemistry
University Medical Center of the Johannes Gutenberg University
Duesbergweg 6, 55128 Mainz, Germany
E-mail: wmueller@uni-mainz.de; wang013@uni-mainz.de

Prof. M. Ackermann
Institute of Functional and Clinical Anatomy
University Medical Center of the Johannes Gutenberg University
Johann Joachim Becher Weg 13, 55099 Mainz, Germany

Prof. T. Gerich
Department of Trauma Surgery
Centre Hospitalier de Luxembourg (CHL)
4 rue Ernest Barblé, 1210 Luxembourg, Luxembourg

The ORCID identification number(s) for the author(s) of this article can be found under https://doi.org/10.1002/adfm.201905220.

DOI: 10.1002/adfm.201905220

mentioned, the cambium layer is highly vascularized and hence highly perfused with blood. There, one cell type is present that is very rich in polyP, the blood platelets,[7] as well in bone cells.[8] In these cells polyP is deposited in the insoluble form as Ca-polyP particles that can be fabricated by a biomimetic process.[9] In general the platelets have been proven to be mitogenic for periosteum-derived cells.[10] The inorganic physiological polyP is solely composed of orthophosphate units that are enzymatically released after hydrolysis catalyzed by the alkaline phosphatase (ALP). In turn the orthophosphate units serve as substrate for the bone forming machinery.[11] Together with Ca^{2+}, calcium phosphate scaffold allows the embedding of bone-like cells which subsequently support the regeneration of functional periosteum-like tissue.[12] Interestingly, the carbonate/phosphate ratio in the bone mineral increases with progressing bone fracture propensity,[13] especially in low turnover bones of aged rats[14] and in necrotic bone.[15]

Interestingly, on the basis of our recent findings, Ca-carbonate is the immature precursor form of the mature hydroxyapatite crystals (a Ca-phosphate mineral)[16,17] that are most likely formed on Ca-carbonate bioseeds by a nonenzymatic phosphate versus carbonate exchange. Ca-carbonate bioseeds are enzymatically deposited in the presence of the carbonic anhydrase.[18] As a consequence of those data it appears to be highly indicated also to test polyP, in concert with the ALP, as an inducer for the maturation of Ca-phosphate in the bone mineral in vivo. Those animal studies have been performed and revealed that biomimetically fabricated Ca-polyP nano-/microparticles[19,20] are superior to other calcium phosphate-based implant materials.

During bone formation as well as during mechanical stimulation of bone cells ATP is increasingly released.[21] Additionally, it could be demonstrated that ATP, as a donor of metabolic energy, is needed to maintain cell homeostasis and bone mineral deposition.[22] More recently our group disclosed that after enzymatic hydrolysis of polyP at the high-energy acid anhydride linkages between the orthophosphate units, the ATP levels increase both intracellularly and extracellularly.[23] In turn, we proposed that polyP particles released in the extracellular space from the blood platelets act as storage for metabolic energy that is released during ALP hydrolysis.[24]

In a dual strategy we propose in the present study that, based on the experimental data available, bone repair can be enhanced by bone grafts that are biomimetically processed with polyP and function as bone augmentation grafts. We report on a convenient procedure to biologize allogeneic human bone parts with a layer of Ca-polyP, comprising microparticles that enhance the morphogenetic activity of the bone samples. The in vitro studies have been performed with SaOS-2 cells, representing a cell line that has properties of osteoblasts, like mineralization.[25–27] Future studies will be performed that are targeted on the development of an artificial periosteum that has been functionalized in a bioinspired way with polyP.

2. Results

2.1. Coating of the Femur Samples with polyP

Human femur samples (thickness of 3 mm) were cut from the mid-shaft region and decellularized as described in the "Experimental Section" (**Figure 1**). Then the samples remained either as unprocessed control ("cortex") or as phosphate-buffered saline (PBS) sample ("cortex-PBS"). The coating of the bone samples with Na-polyP was performed by submersing into a 20 mg/mL Na-polyP solution followed by air-drying ("Na-polyP" coat). The coating of the cortex samples with Na-polyP and $CaCl_2$ was performed under $CaCl_2$:Na-polyP ratio conditions as described.[9] From these studies it is known that amorphous Ca-polyP particles are formed, if $CaCl_2$ is added at over-stoichiometric concentration ratios. These bone samples are termed "Ca-polyP-MP" coat.

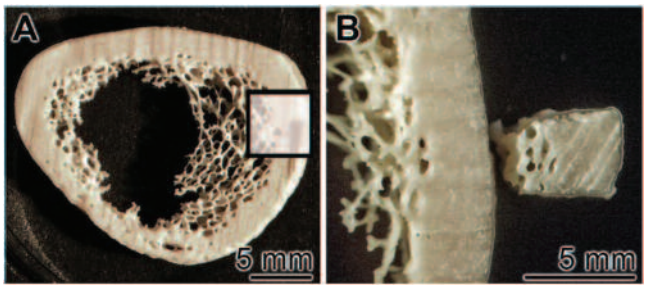

Figure 1. Preparation of the human femur samples. A) The bone was decellularized and cubes with an edge length of 3 mm were cut out (marked). B) Details from (A).

The surface of the control samples, inspected by ESEM, disclosed the stacked stocks of the mineralic bone units that leave open space for the organic fibrillous and nonfibrillous material that has been removed during decellularization (**Figure 2**A–D). After treatment with Na-polyP, the processed bone specimens, "Na-polyP" coat, show already a closure of most of the openings, fissures and gaps (Figure 2E–H). A likewise smoothing and filling of the gaps, previously existing on the surface of the "cortex" and also "cortex-PBS" samples, is seen onto "Ca-polyP-MP" coat samples (Figure 2I–L). However, already by ESEM analysis it becomes overt that the surface of these specimens is structured and comprises particles that are embedded into the Ca-polyP coat (Figure 2L). At a higher magnification those particles turned out to be densely arranged within the polyP coat. Like in the previous study[28] those globular particles with an average diameter of 155 ± 92 nm ($N = 20$) have been formed in situ within the Na-polyP layer onto the bone after the $CaCl_2$ treatment (**Figure 3**B).

The surface roughness was assessed microscopically and computed by the root mean square (RMS). The uncoated ("cortex") bone yielded a roughness of 26–40 nm (mean 33 ± 7 nm), while the polyP coated bone specimens had roughnesses of 19–31 nm (mean 25 ± 6 nm) and 16–32 nm (mean 24 ± 8 nm), respectively. The difference between the controls (uncoated) and the polyP-coated bone specimens is significant ($p < 0.05$).

No strong size difference is seen between the microparticles formed in situ within the Ca-polyP layer onto the bone sample, "Ca-polyP-MP" coat (Figure 3B), and the template-free particle Ca-polyP-MP formation (Figure 3A); particles with a size of 205 ± 57 nm are measured. The difference is only seen in the bone/hydroxyapatite template that embeds the particles onto their surface (cortical bone).

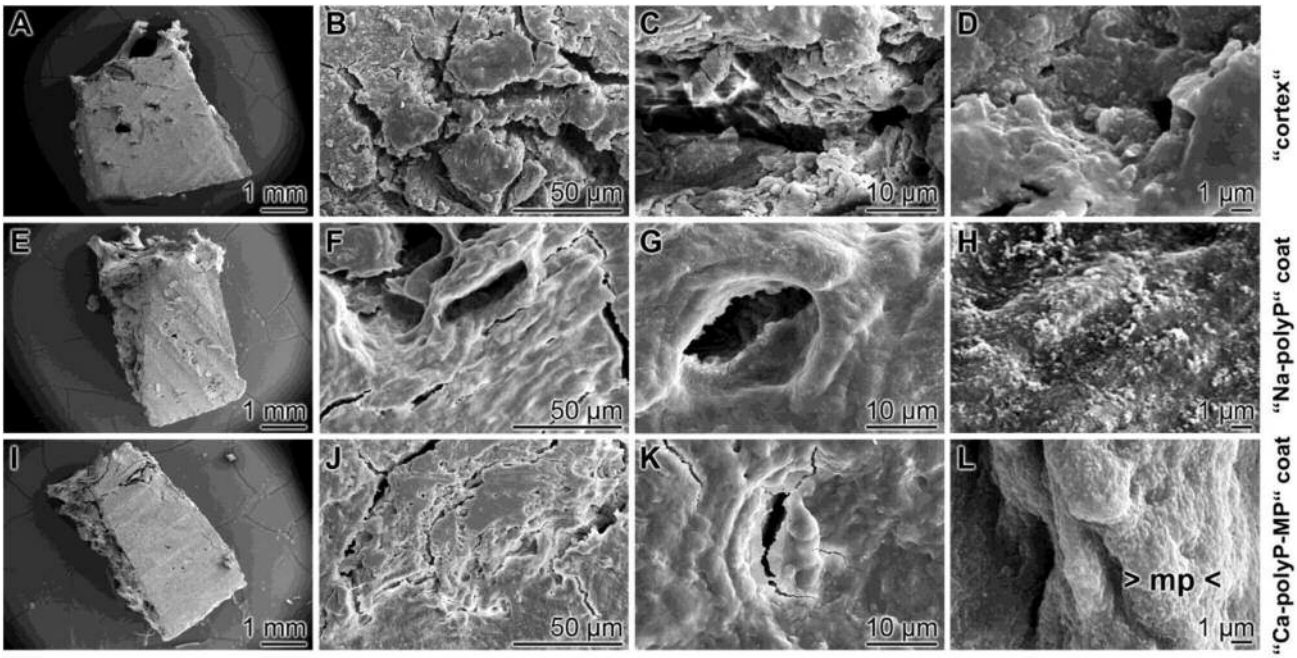

Figure 2. Coating of the cortical/compact bone specimens; ESEM. A–D) Control bone "cortex" samples. E–H) The cortical/compact specimens were treated with Na-polyP alone, the "Na-polyP" coat. In contrast to the control samples, the ones with the "Na-polyP" coat already show a closure of most of the gaps between the mineralic bone parts, previously harboring the organic bone constituents. I–L) Bone samples treated first with Na-polyP and subsequently with $CaCl_2$; "Ca-polyP-MP" coat. The surfaces of the samples are smooth and leave open small fissures. At higher magnification the rippled surface disclose microparticles (>mp<).

2.2. Characterization of the polyP Coat, Layered onto the Bone Specimens

The samples were characterized both with chemical and biomechanical methods.

Energy Dispersive X-Ray Spectroscopy (EDX) Analysis: The comparative experiment was performed with unprocessed cortical bone (**Figure 4**A,B) as well as with Ca-polyP coated specimens, "Ca-polyP-MP" coat (Figure 4C,D). The ESEM image for the control bone sample "cortex" is given (Figure 4A). In parallel the EDX spectrum has been recorded (Figure 4B); it shows distinct signals for the elements O, P, and Ca. For the "Ca-polyP-MP" coat sample with its characteristic polyP layer, composed of closely arranged microparticles (Figure 4C), a qualitatively similar EDX spectrum was recorded as well (Figure 4D). However, a striking difference exists with respect to the Ca:P ratios between the two samples, as assessed by semiquantitative EDX determinations. While the bone sample shows with 1.52 ± 0.32:1 (Ca:P ratio) a value characteristic for human bone,[29] the respective ratio for Ca:P was determined

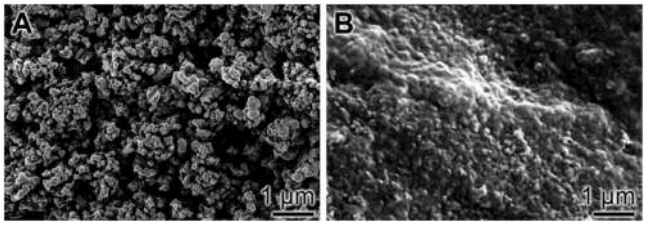

Figure 3. Comparison between A) Ca-polyP microparticles, "Ca-polyP-MP," formed without any template, SEM; and B) Ca-polyP microparticles, formed in situ within the polyP layer after addition of $CaCl_2$, ESEM.

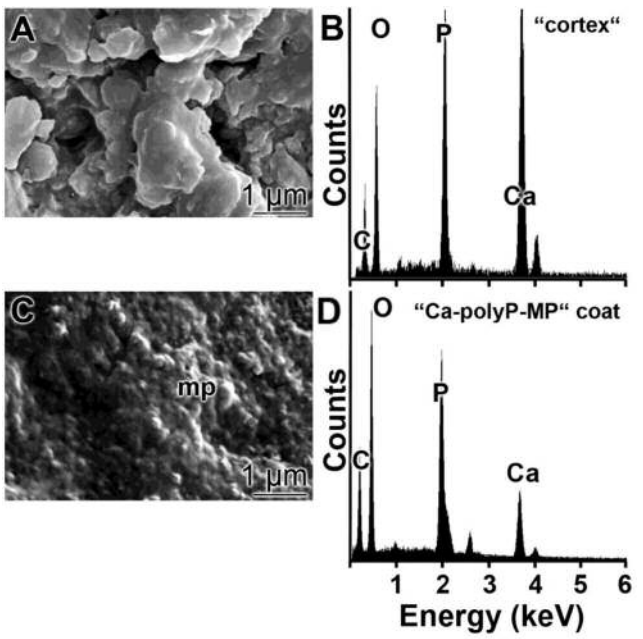

Figure 4. EDX spectra of the bone surface in the control ("cortex") (B) as well as in the polyP coated "Ca-polyP-MP" (mp) coat material (D) together with the corresponding ESEM images (A and C). In the control spectrum the signal for Ca is significantly higher, in relation to the one of P, compared to the one measured for the polyP coated bone.

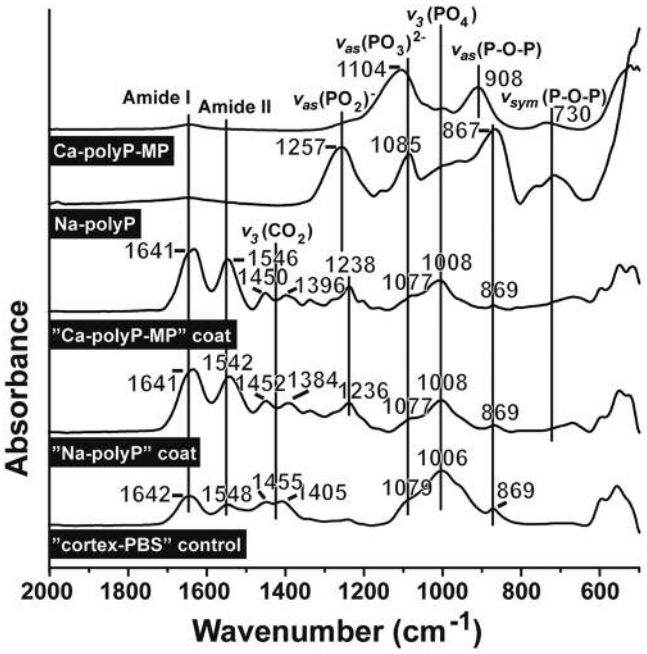

Figure 5. The FTIR spectral characteristics for the polyP reference samples (Ca-polyP-MP and Na-polyP) as well as the untreated bone ("cortex-PBS") and the polyP coated bone samples ("Ca-polyP-MP" coat and "Na-polyP" coat) are shown. The characteristic signals for polyP with $\nu_{as}(PO_2)^-$, ν_{as}(P-O-P), and ν_{sym}(P-O-P) are aligned. Also the bone-specific vibrations for Amide I and Amide II are marked.

to be with 0.78 ± 0.24:1 in the range previously determined for Ca-polyP microparticles.[9] This result is taken as an additional proof that the bone samples are coated with polyP.

X-Ray Diffraction (XRD) Pattern: The diffraction pattern, collected from particles prepared with the same method applied for coating of the bone samples, with a super-stoichiometric ratio between $CaCl_2$ and Na-polyP showed no distinct sharp diffraction peak(s), indicating that the material is amorphous (data not shown).

Fourier-Transform Infrared (FTIR) Spectroscopy: The FTIR spectra support that the polyP-treated bone samples are indeed supplemented with the polymer (**Figure 5**). The reference spectra of the Ca-polyP-MP particles, as well as of Na-polyP, show the characteristic signals for polyP with ν_{as}(P-O-P) at the wavenumber of ≈900 cm^{-1} and with symmetric ν_{sym}(P-O-P) at ≈730 cm^{-1} vibrations, as well as the $\nu_{as}(PO_2)^-$ at ≈1240 cm^{-1}. In addition, the $\nu_{as}(PO_3)^{2-}$ (≈1080 cm^{-1}) and $\nu_3(PO_4)$ (≈1005 cm^{-1}) reflect the phosphate vibrations of the polymer. In contrast, the bone signals in both the "Na-polyP" coat and the "Ca-polyP-MP" coat as well as the "cortex-PBS" are found at ≈1641 cm^{-1} (Amide I), ≈1545 cm^{-1} (Amide II), and at ≈1450 cm^{-1} ($\nu_3(CO_2)$). In the bone coated samples, "Ca-polyP-MP" coat and "Na-polyP" coat, the polyP-characteristic vibrations for $\nu_{as}(PO_2)^-$ at ≈1240 cm^{-1} and ν_{sym}(P-O-P) at ≈730 cm^{-1} are seen, while the others are covered. These polyP coated samples indicate also the presence of the bone by highlighting the Amide I and Amide II vibrations.

Nanoindentation: The nanoindentation measurements were performed as described in the "Experimental Section." Representative load/displacement curves for the different bone samples are depicted in **Figure 6**. The respective values for the

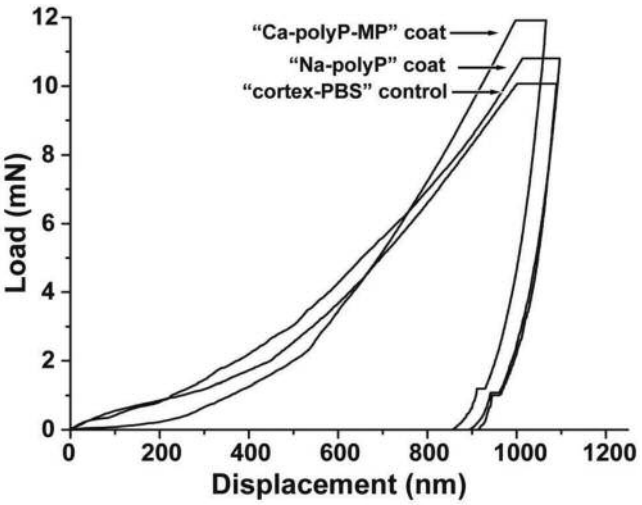

Figure 6. Characteristic load-displacement curves from indentation experiments with a control "cortex" sample, as well as the samples with the polyP coatings the "Na-polyP" coat and the "Ca-polyP-MP" coat.

Martens hardness (HM) as well as the elastic modulus (E) were calculated applying the Nano-Test Platform Four V.40.08 software package. The recordings show that the "Ca-polyP-MP" coat has an increased hardness compared to the "Na-polyP" coat and also the "cortex-PBS" control. This conclusion bases on the observation that the diamond indenter requires a higher force (12 mN) to reach to the desired indentation depth of 1000 nm. In comparison, for the "Na-polyP" coat (10.9 mN) and "cortex-PBS" control (10.1 mN) lower forces are needed. These observations are supported by the calculated values for HM, which are highest for the "Ca-polyP-MP" coat (0.46 ± 0.12 GPa; n = 40), followed by the "Na-polyP" coat (0.4 ± 0.17 GPa; n = 40) and the "cortex-PBS" control (0.39 ± 0.14 GPa; n = 40). Focusing on the descending unloading parts of the respective load/displacement curves, which are almost rectangular to the abscissa x-axis (Figure 6), it can be deduced, that all three materials display only minimal elastic recovery properties. This observation is in agreement with the calculated values for the elastic modulus which do not differ significantly between the three sample materials ("Ca-polyP-MP" coat: E = 19.12 ± 4.55 GPa, "Na-polyP" coat: E = 18.33 ± 6.84 GPa, "cortex-PBS" control: E = 19.88 ± 4.66 GPa; n = 40). Taken together, the polyP based coatings do not alter the elastic surface properties, but in case of the Ca-polyP-MP treatment a significant increase in hardness is recorded.

2.3. Effect on Cell Growth and Mineralization

The effect of polyP both on cell growth and on bone biomineral formation (hydroxyapatite-like material) was determined in SaOS-2 cells. This cell system, in contrast for the growth studies on hydroxyapatite/bone, allows quantitative results.

Effect on Cell Growth: The cell viability/growth was determined by the methylthiazolyldiphenyl-tetrazolium bromide (MTT) assay. The values determined in the polyP-non-existent were set to 100%. The data revealed (**Figure 7**) that during a

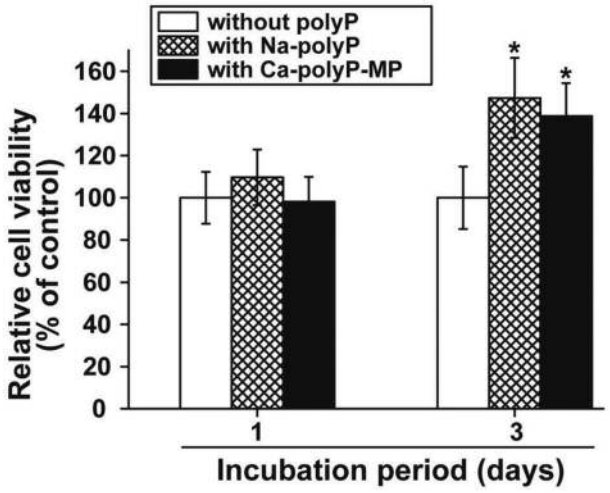

Figure 7. Viability of SaOS-2 cells determined during a 1 and 3 d incubation period, using the MTT assay system. The cultures remained either without polyP (controls; "cortex-PBS") or with 50 µg mL^{-1} of "Na-polyP" coat or "Ca-polyP-MP" coat. The values are expressed as percent growth over control (set at 100%). The number of parallel experiments was 10. Data are means ± SD (*$p < 0.05$).

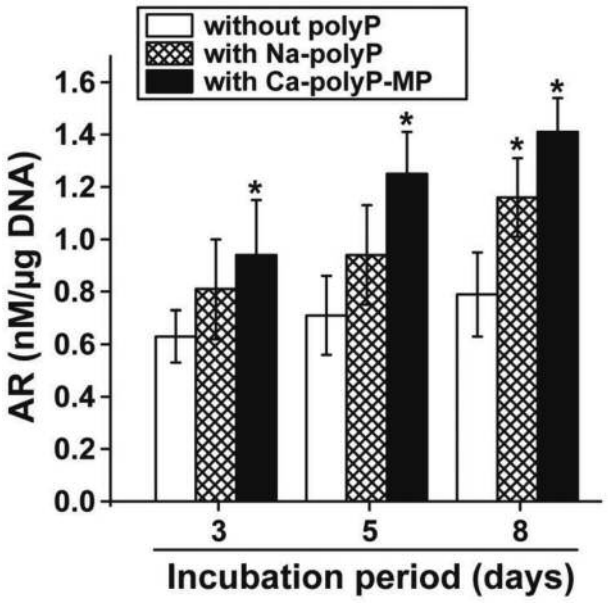

Figure 8. Formation of hydroxyapatite-like deposits onto SaOS-2 cells, as measured with alizarin red S (AR). The cells were incubated without polyP (controls; open bars), or in medium/serum supplemented with 50 µg/mL of either Na-polyP (cross-hatched) or Ca-polyP-MP (solid) for a period of 3 d. Then, the cells were continued to be cultivated for 3–8 d in medium/serum, with the MAC. Finally, the cells were collected and an extract prepared from them which was reacted with alizarin red S. Subsequently spectroscopic determination was performed as described in the "Experimental Section." The extent of biomineralization is correlated with the DNA content in the assays to normalize for the cell number. Values represent the means (± SD) from 10 separate experiments each (*$p < 0.01$)

one-day incubation period the growth of the cells was not significantly different in the assays, irrespectively of the presence of polyP. However, after the 3 d incubation the cell growth/viability in the polyP-containing series was significantly higher with ≈40%.

PolyP-Induced Mineralization in SaOS-2 Cells: At the beginning of the experiment the cells were incubated in the absence of MAC for 3 d without any polyP component or were exposed to 50 µg mL^{-1} of either Na-polyP or of Ca-polyP-MP. Then MAC was added to the assays and incubation was continued for additional 3–8 d. Then a quantitative assessment of the production of hydroxyapatite-like deposits in SaOS-2 cells was performed with the anthraquinone dye alizarin red S, applying a spectroscopic technique (**Figure 8**). The values for the respective optical densities measured were correlated with the cell number, as measured by DNA concentration in the assays. In the absence of polyP the value for the alizarin red S increased to 0.63 ± 0.11 nM μg^{-1} DNA, a value which did not significantly changed during the 3–8 d incubation period with MAC. However, the polyP-exposed cultures produced more hydroxyapatite-like deposits; the increase in the assays with Na-polyP became statistically significant after 8 d with 1.15 ± 0.16 nM μg^{-1} DNA. In the assays with Ca-polyP-MP the increase was already significantly higher, compared to the assays in the absence of polyP, after 3 d (0.94 ± 0.21 nM μg^{-1} DNA) and increased further during the complete incubation period of 8 d (1.41 ± 0.13 nM μg^{-1} DNA).

2.4. Attachment of the Cells onto the Bone Matrices

At outlined above (Figure 7) the SaOS-2 show an increased growth/proliferation in the MTT assay if exposed to "Na-polyP" coat or to "Ca-polyP-MP" coat. To verify that the cells also attach to both the untreated bone samples ("cortex") and to the polyP coated bone specimens, "Na-polyP" coat as well as "Ca-polyP-MP" coat, the bone fragments were incubated together with the cells. After a 3 d incubation period, the samples were taken out and the cells were stained with Calcein AM to identify living cells on the bone samples. After inspection with fluorescence light it becomes overt, that the number of cells attached onto the untreated sample is considerably lower (**Figure 9**A), compared to those that are visualized onto the "Na-polyP" coat (Figure 9B) or the "Ca-polyP-MP" coat (Figure 9C).

The surface of the demineralized cortical human bone, like the "cortex" samples, shows a crystal-like morphology with thin and elongated lacunae along the tangential direction; very often also Haversian canals. These structures are also seen if the "Na-polyP" coat bone specimens are analyzed by ESEM at time zero or after 2 h (**Figure 10**A,C). However, if those samples are incubated in medium/serum for >2 h, the well-defined radial structures with their deep contours within the Haversian system disappear (Figure 10E). At higher magnification, those surfaces appear, in contrast those of the unprocessed controls (Figure 10B), as a smooth layers (Figure 10D). After an additional 2 h incubation in medium/serum, the surfaces of the Na-polyP treated bone specimens become very plain (Figure 10E). At higher magnification small—about 15 nm large—granules become visible that are already reminiscent to the polyP coacervate (Figure 10F).[30] From these data it might be suggested that the Na-polyP constituent in contact with the bone material

Figure 9. Abundance of SaOS-2 cells onto A) nontreated "cortex" bone samples, B) "Na-polyP" coat processed bone specimens, or C) "Ca-polyP-MP" coat treated bone. After an incubation period of 3 d the cells were stained with Calcein AM and inspected by fluorescence microscopy.

undergoes coacervation, as a results of a contact of the polymer with peptides/proteins that are present in the serum.

In the experiments with SaOS-2 cells the different bone specimens were exposed to medium/serum and incubated. In the first series, the samples remained in the culture medium/serum for 1 d. Then the different samples were inspected by ESEM after glutaraldehyde/osmium oxide fixation and critical point drying (**Figure 11**). The images show that the cells attached to the untreated bone, "cortex," are nesting in the cavities of the deeply furrowed plain bone surface (Figure 11A,B). In contrast, the cells in the assays with the "Na-polyP" coat specimens are not globular but show a spreading appearance (Figure 11C,D). Analyzing the attachment pattern of the SaOS-2 cells on the surfaces of the "Ca-polyP-MP" coat bone specimens after the 1 d-incubation period the cells appear to be entrapped into the polyP-coacervate (Figure 11E,F). The coacervate phase of the polyP can be deduced from the smooth and gel-like consistence of the polyP layer onto the bone substratum.

If the cells are incubated for the longer, 3 d, incubation period onto the bone control, "cortex" (**Figure 12**A), or the polyP coated specimens, "Na-polyP" coat (Figure 12D) as well as the "Ca-polyP-MP" coat (Figure 12 G), the polyP smooth coat has been absent in the latter samples, due to the dissolution of the coacervate. The morphology of the cells, residing in the bone cavities, is now unified and globular-shaped. The only distinctive feature between the samples is the density of the cells; the lowest one is seen in the "cortex" samples (Figure 12B,C), in comparison to the cell densities onto "Na-polyP" coat (Figure 12E,F) and "Ca-polyP-MP" coat (Figure 12H,I).

3. Discussion

While bone growth in length is primarily directed by chondrocytes within the proliferative and hypertrophic zones of the growth plate, bone thickening is driven by cells of the periosteum that mediate periosteal bone mineral apposition (reviewed in ref. [31]). The periosteum tissue its their derived cells elicits osteogenic potential[32] and is causatively involved in bone regeneration and repair of the outer (periosteal) bone surface.[33] It has been proposed that the limited healing of bone allografts can be attributed to the impairment or devitalization/removal of the periosteum with its osteogenic cells and the osteoinductive signals released from them.[32] As outlined in the "Introduction" the periosteum contains specific stem cells that, like the bone marrow stromal cells/skeletal stem

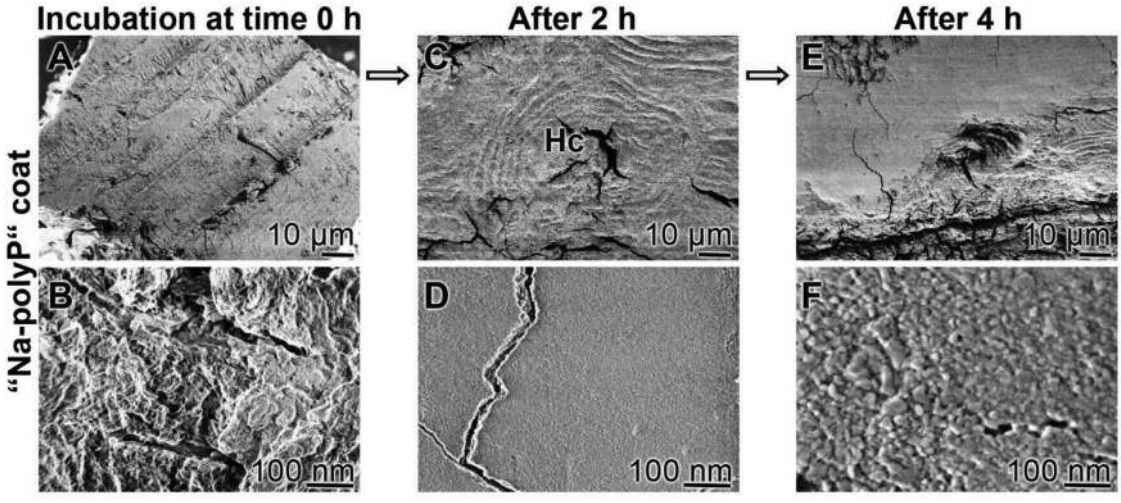

Figure 10. Change of the surface morphology of the "Na-polyP" coat bone samples during incubation in medium/serum; SEM. A,B) Prior to the transfer into culture medium/serum (time 0 h), the surfaces of the samples are crystal-like and traversed with thin and elongated lacunae. C,D) After incubation in medium/serum for only 2 h only smooth surfaces are recognized. Haversian canals (Hc) with only less deep contours are seen. E,F) After a 4 h incubation the very plain surfaces remain. At higher magnification (F) small—about 15 nm large—granules become visible that are indicative for a polyP coacervate.

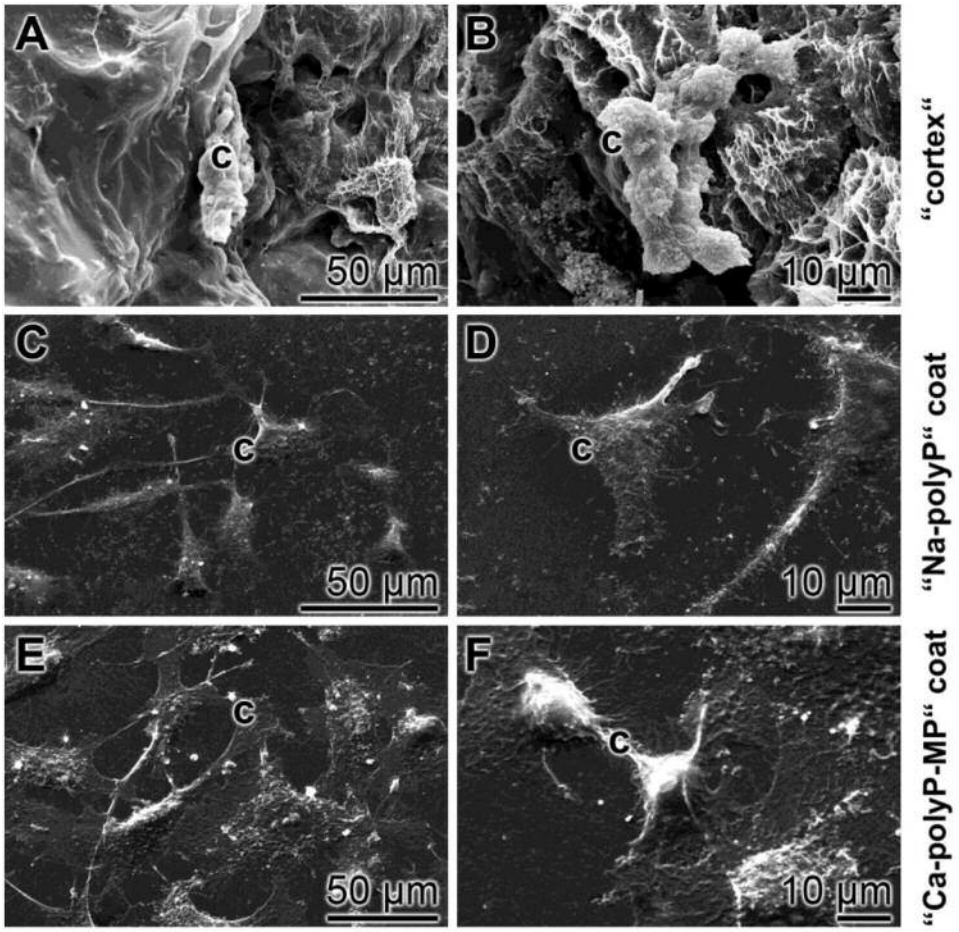

Figure 11. Attachment and growth of SaOS-2 cells (c) onto the different bone fragments, after a 1 d incubation; ESEM. Cells onto A,B) unprocessed bone, the "cortex," are nesting in the rutted crystal-like surface; onto C,D) the "Na-polyP" coat overlayed bone surface are flat and spreading; onto E,F) "Ca-polyP-MP" coat samples appear as being coated within polyP coacervate.

cells, derive from a common embryonic mesenchymal lineage but display both a greater clonogenicity and increased growth and differentiation potential than the skeletal stem cells.[34] These periosteal cells synthesize and secrete with periostin an osteoblast-specific factor that is crucially involved in bone repair. Interestingly, the function of periostin, a ligand for α-V/β-3 and α-V/β-5 integrins, is correlated with the basal energy expenditure in adipose tissue of aging mice.[35] It has been shown that the expression of periostin is markedly decreased in aged brown and white adipose tissue depots. Furthermore, an increase in ATP production in bone cells, producing bone mineral deposits, accelerates the fracture healing process.[36] The correlation between energy consumption and bone mineralization is also underscored by the finding that the level of the RNA-binding protein Lin28a in osteoprecursor cells is positively correlated with the level of the ALP, as well as the extent of alizarin red-positive cells/mineralization, the calcium content, and the proliferation/differentiation potency of these cells.[37] In addition, it is established that glycolysis, as the major metabolic pathway for ATP generation also needed for osteoblast differentiation and function, significantly contributes to the cortical modeling by the bone mineralizing cells of the periosteum.[38]

Autologous (autogenous) bone grafts is still the gold standard in implantology,[39] while decellularized allografts are less functionally active but stimulate mesenchymal stem cell proliferation and osteogenic differentiation both in vitro and in vivo to some extent, and in turn are considered as effective and promising biological bone grafts.[40] Therefore, efforts have been undertaken to biologize those bone materials, e.g. by wrapping those implants with hydrolytically degradable hydrogels containing stem cells to mimic the periosteum,[32] or to revitalize the bone with an engineered periosteum, comprising periosteal factors.[41]

In our strategy to fabricate a tissue-engineered periosteum, we used allogeneic decellularized bone samples from human femur and biologized them with polyP. The rationale behind was to use this physiological inorganic polymer, existing in every cell type of humans,[7,8] as a morphogenetic additive for the relatively inert allogeneic bone specimens. In previous studies polyP was found to be morphogenetically active, meaning it induces the expression of those proteins/enzymes that are required for anabolic pathways in cell proliferation, differentiation and function (reviewed in ref. [42]). Among them is the ALP,[43] an enzyme that hydrolytically cleaves the polymer in a processive manner.[44] Furthermore, the ALP is

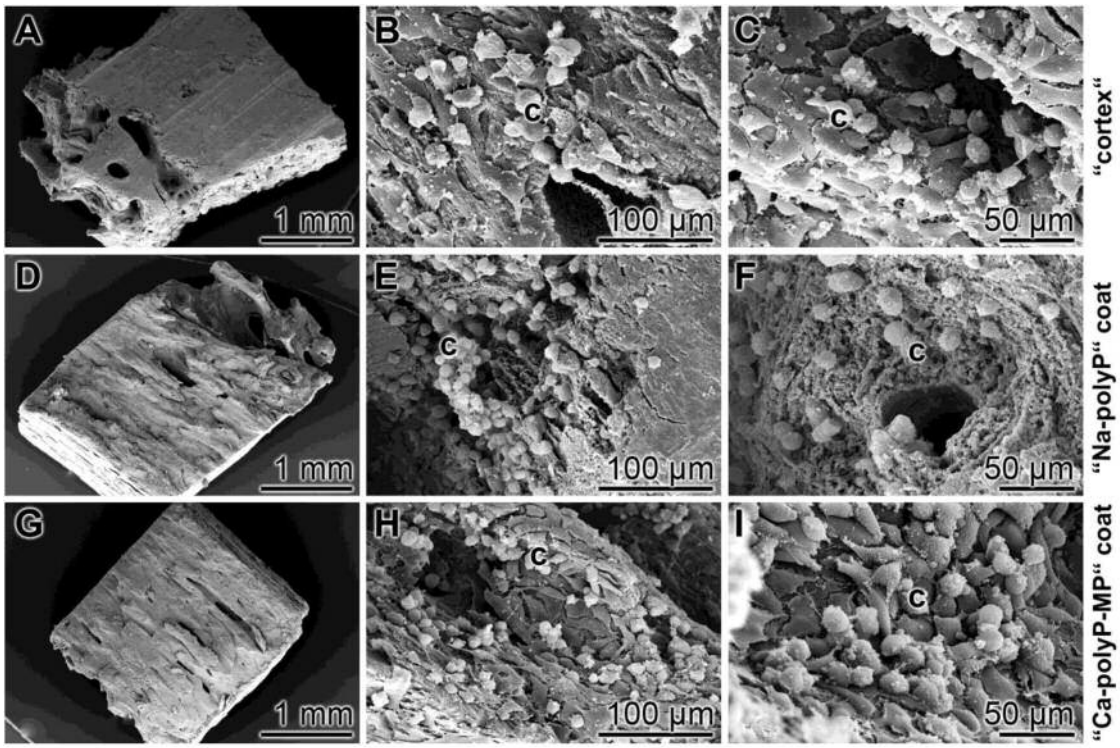

Figure 12. Distribution pattern of SaOS-2 cells (c) onto A–C) "cortex," D–F) "Na-polyP" coat, as well as G–I) "Ca-polyP-MP" coat; ESEM. After the 3 d incubation the morphology of the cells, cultured onto the three different bone supports, is not different. Only the density of the cells is apparently higher onto the polyP coated bone specimens.

that enzyme which has been considered to hydrolyze pyrophosphate, accumulating during bone formation.[45] Importantly, experimental evidence has been presented revealing ADP/ATP pools to be upregulated both intra- and extracellularly after ALP mediated polyP hydrolysis.[46] It has been proposed that, thereafter, the formed ADP becomes phosphorylated to ATP via the enzyme adenylate kinase.[47] In turn, ATP acts extracellularly as a chemotaxis signal for endothelial cells during the initial phases of microvascularization.[46,48] Importantly, Na-polyP has been fabricated into Ca-polyP nano-/microparticles which are amorphous, applying a biomimetic process.[9] This storage form undergoes coacervation after having contact with peptides/proteins and, by that, becomes functionally active.[30] While Ca-polyP has a growth stimulatory effect on bone cells both in vivo and in vivo, Ca-phosphate is involved primarily in the regulation of the differentiation of osteoblasts and the osteoblastic lineage via the IGF-1 and ERK1/2 pathways, and also in the increased steady-state-expression of BMPs (see refs. [42,49]).

In the present study bone samples were incubated in a Na-polyP solution in order to allow a coating of the bone samples. The binding of polyP to the surface of the bone samples most likely takes place via Coulomb interaction (formation of salt linkages) between the negatively charged phosphate groups of the polyP molecule and the positively charged calcium ions at the hydroxyapatite crystal surface as it is assumed also for other anionic macromolecules.[50] During this process a Na^+ to Ca^{2+} exchange can be postulated based on analytical data, revealing that the Ca/P molar ratio of bone can range from 1.15 to 1.70, depending on the nutritional status of the individual.[51] Likewise, in osteoporotic individuals the Ca/P molar ratio is even lower than normal.[52] This finding implies that the Ca/P ratio in bone is usually lower than theoretical value for pure hydroxyapatite.[53] As a consequence "foreign ions" can intrude into the bone Ca-phosphate deposits, like Mg^{2+}, Na^+, K^+, Cl^- and F^-.[54] Such an infiltration of Na^+ is also assumed to occur after submersion of the bone sample in Na-polyP solution, the "Na-polyP" coat. It is known that sodium ions, in contrast to potassium ions, are able not only to displace ions in the hydration layer of hydroxyapatite crystals, but also to penetrate and to exchange with Ca^{2+} ions from the crystal surfaces.[55] In principle, the Na^+ ions from the Na-polyP could exchange with Ca^{2+} ions both from the hydration shell and from the surface or the interior of the bone/hydroxyapatite crystal structure. It is assumed that these ion exchanges most likely involve the hydrated shell and the surface of the bone hydroxyapatite crystals.[55] In order to maintain electroneutrality[56] one Ca^{2+} ion should be replaced by two Na^+ ions, but it cannot be excluded that due to space restrictions (both ions have similar radii; Na^+, 0.95 Å; Ca^{2+}, 0.98 Å)[55] the position of one Ca^{2+} ion will become replaced by less than two Na^+ ions entering the crystal surface, resulting in a change of the net charge of the bone/hydroxyapatite crystal.[57]

The determination of the element composition of the Na-polyP overlay on top of the bone sample by FTIR spectroscopy confirmed the existence of polyP within the Ca-phosphate bone matrix, especially based on the $\nu_{as}(PO_2)^-$ and ν_{as}(P-O-P) vibrations. The bone matrix was identified by the Amide I and Amide II signals.[58] During this processing with

Na-polyP the biomechanical properties of the bone samples did not change, both with respect to the hardness and the creep value.

In a subsequent step the polyP-infiltrated bone samples were incubated with $CaCl_2$. Interesting, within the surface layer Ca-polyP microparticles are formed in situ onto the bone matrix ("Ca-polyP-MP" coat), showing a morphology and a size similar to those visualized for particles prepared in the absence of a bone support.[9] The in situ formed Ca-polyP particles are slightly larger (with 205 ± 57 nm) than those that had been fabricated alone from Na-polyP and $CaCl_2$ (≈100 nm); we attribute this size differences to the effect of (in)organic constituents of the bone specimens during the in situ particle formation. In those polyP layers around the bone specimens the polyP FTIR signals were recorded. The in situ formed polyP particle technology provides a higher immobilization potential at the bone specimens than the use of only physically attached polyP particles. This is especially useful for a potential application in restorative medicine in the future. Surprising was the finding that the Martens hardness of those "Ca-polyP-MP" coat bone sample was slightly, but insignificantly, higher. As demonstrated in previous studies, the SaOS-2 cells that had been cultured together with Na-polyP or Ca-polyP-MP showed, after a 3 d incubation period an about 30% higher growth rate than the controls.[9] Similarly, the potency of SaOS-2 cells to form mineralic deposits significantly increased after exposure to Na-polyP and Ca-polyP-MP during the 3 d to 8 d incubation period.

In a separate series of experiments the attachment behavior of the cells was documented by both light (fluorescence) and electron microscopy. Inspection after 3 d by fluorescence microscopy revealed that the number of cells attached to the plain surface is considerably higher, compared to control, in the polyP coated bone samples (both "Na-polyP" coat and "Ca-polyP-MP" coat).

After a 2 h to 4 h incubation of the "Na-polyP" coat bone samples in medium/serum a transformation of the polyP coat to a coacervate layer occurs. This transformation has already been documented to happen in a previous study,[30] if polyP particles or layers are transferred to an aqueous milieu, containing peptides/proteins. This coacervate phase was found to be the functional active morphogenetic stage of polyP.

After addition of cells to the bone system, and incubation for 1 d in medium/serum, it could be documented that SaOS-2 cells attach to the bone within the crystal cavities with a globular morphology. In contrast, the cells attached to the polyP coated bone matrices, both with a "Na-polyP" coat and a "Ca-polyP-MP" coat, show altered cell morphologies. These cells show an actively metabolizing spreading pattern,[59] with long protrusions and interspersed retractions. It appears, especially in the assays with "Ca-polyP-MP" coat that the cells have been enveloped in a polyP coacervate coat. After 3 d of incubation the coacervate-like layer disappeared and allowed the cells, now showing a globular morphology in all assays, to settle and grow in the crystal-like nests.

4. Conclusion

In conclusion, based on the substoichiometric molar ratio of Ca/P in bone, this organ can incorporate Na^+ into its scaffold, as schematically outlined in **Figure 13**A. In the first step, a surplus of free negative ion valences exists in bone (Figure 13A-1). To reach an equilibrium a thermodynamic flow of Na^+ from the Na-polyP coat into the bone matrix may proceed (Figure 13A-2), allowing a tight layering of a polyP coat onto the bone surface. While the bone is enriched with Na^+, the polyP overlay becomes deprived of Na^+ (Figure 13A-3). To compensate for this deficiency the bone specimens, together with the overlayed Na-polyP, are transferred to a $CaCl_2$ solution (Figure 13A-4). A near ionic equilibrium is reached and a higher biological functionality is reached. The bone samples provide a superior platform for the cells to adhere, with the consequence of an increased growth rate.

In the future, Na-polyP will be applied in a hydrogel to utilize its bone repair potency as a guiding matrix for the regeneration of the periosteum (Figure 13B). The planned steps, here demonstrated in the femoral region of a human cadaver, are as follows. A surgical incision is performed, opening the subdermal region with the adipose tissue (Figure 13B-1). After the periosteal surgical sectioning the bone damage shows up (Figure 13B-2). Then, Na-polyP dissolved in a hydrogel will be injected into the subperiosteal cavity near the bone defect (Figure 13B-3). In the last step, the periosteal ends will be superimposed over the bone and covered with a polyP-enriched biological membrane, fabricated from compressed collagen, acting as a graft-like membrane for separation of the dermal tissue layer (Figure 13B-4).

5. Experimental Section

Materials: Na-polyphosphate (Na-polyP) with an average chain length of 40 phosphate units was purchased from Chemische Fabrik Budenheim (Budenheim; Germany).

Preparation of Nano/Microparticles: Calcium polyP microparticles (termed Ca-polyP-MP) were prepared from Na-polyP as described.[9]

Decellularized Human Bone Samples: Human cadaver femurs were provided by the Institute of Functional and Clinical Anatomy, University Medical Center of the Johannes Gutenberg University, Mainz, Germany, following the ethical guidelines of the University Medical Center Mainz. Those samples had been used for all experiments mentioned here. The cross sections through the mid-shaft of femurs were prepared having a height of ≈3 mm. The samples were processed as described;[40] in brief, femur samples were decellularized with 0.5% SDS (sodium dodecyl sulfate; Sigma–Aldrich, Taufkirchen; Germany) and 0.1% ammonium hydroxide (Sigma–Aldrich). Subsequently the specimens were repeatedly washed with deionized water until SDS was completely removed from the matrix. Subsequently, slices with dimensions of 3 mm through the cortical/compact bone region were cut out and used for coating.

Coating of Decellularized Bone with polyP: The bone slices were submersed into a Na-polyP solution (1 g of polyP in 50 mL distilled water; pH 10) for a period of 12 h, while shaking. Then the samples were removed and the nonadsorbed Na-polyP was cleared by very brief dipping onto a filter paper. Some slices remained at this step were briefly washed with distilled water and then air-dried ("Na-polyP" coat). Other slices were placed into a $CaCl_2 \times 2H_2O$ solution (#1.02382 Supelco/Sigma; 3 g $CaCl_2$ in 50 mL water) for another 12 h. Then the samples were briefly dipped into distilled water and then briefly placed onto a filter paper. Finally the samples were air-dried at room temperature and termed "Ca-polyP-MP" coat. Two controls were analyzed in parallel; first, an unprocessed one ("cortex") and second, a slice submersed into PBS which was termed "cortex-PBS."

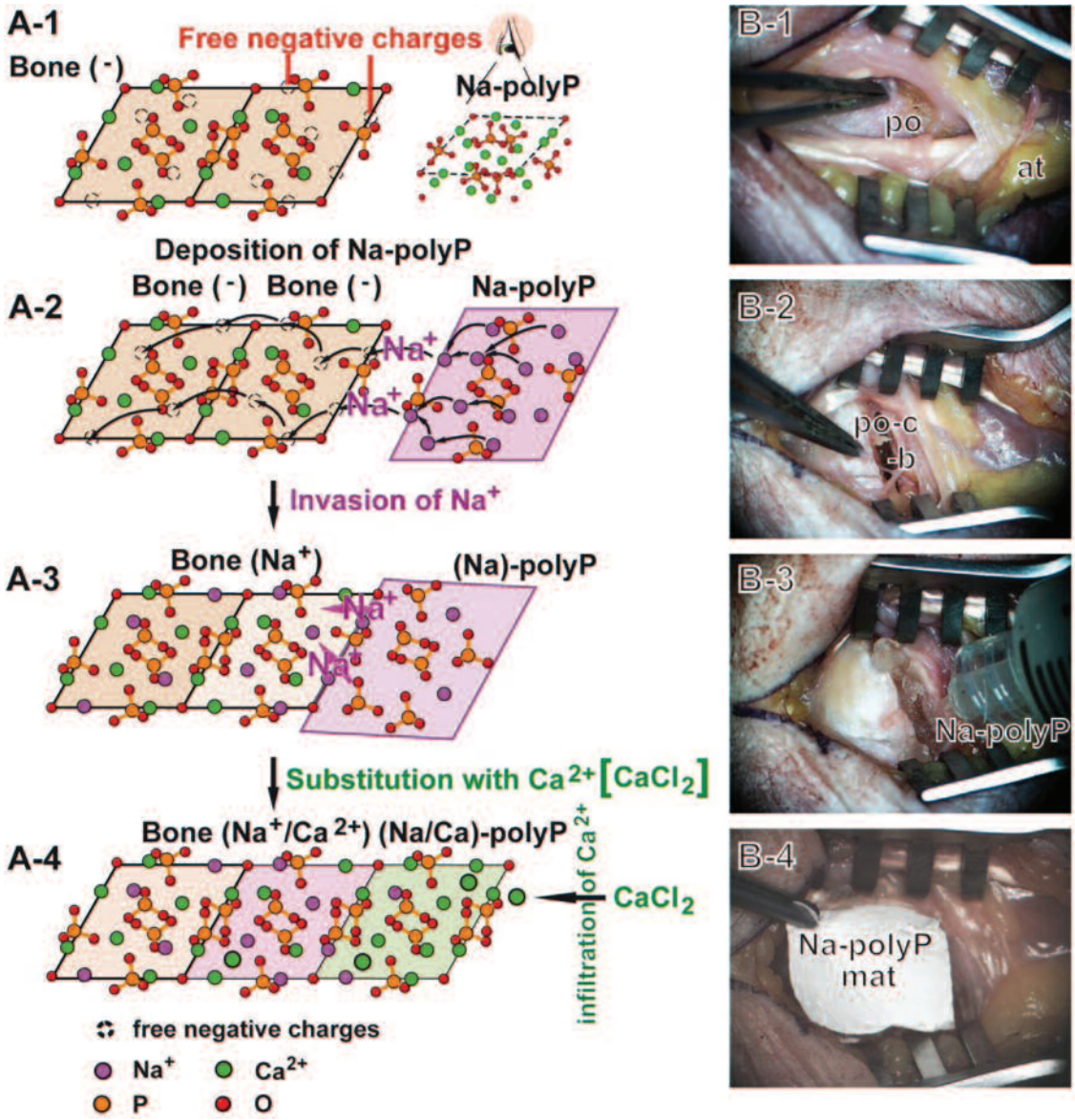

Figure 13. A) Schematic illustration of the cation-driven coating of bone samples with polyP, as well as B) an outline of the planed protocol for exploitation of the regenerative potential of polyP in the periosteal region. Driven by an ionic imbalance between bone and Na-polyP (A-1), Na^+ ions migrate from Na-polyP into bone (A-2,A-3). The resulting shortfall of cations is compensated by $CaCl_2$ (A-4). B) The potential application of polyP with its regenerative potential for bone surfaces is outlined with femurs from a human cadaver. After an incision through the dermis and the adipose tissue (at) down to the surface of the periosteum (po) (B-1) and a subsequent cut of it (po-c) the damaged bone (b) is reached (B-2). The surface of the impaired bone will be treated with a hydrogel, supplemented with polyP (Na-polyP) (B-3). The periosteum will be overlayed above the hydrogel and covered by a Na-polyP containing membrane (Na-polyP mat).

Microscopic Analysis and Surface Roughness: The high-resolution SEM (scanning electron microscope) images were obtained with a Zeiss Gemini 1530 (Zeiss Oberkochem; Germany). For low-resolution ESEM studies an ESEM XL-30 machine (Philips, Eindhoven; Netherlands) was applied.[60] Light microscopical images were taken with a VHX-600 Digital Microscope from KEYENCE (Neu-Isenburg, Germany). The surface roughness of the bone samples was measured with the software provided by the manufacturer. Scans (at least six scans) from 5×5 µm^2 are over a total area of 100×100 µm^2. The root mean square (RMS) was determined as described.[61]

For SEM/ESEM inspection, the cells were transferred into 2% [v/v] aqueous glutaraldehyde fixative, fixated in osmium oxide, processed through acetone dehydration steps and finally critical point dried at 43 °C, as described.[62]

For the incubation of noncoated or polyP coated bone samples in the presence of medium/serum the respective samples, uncoated ("cortex") or polyP coated bone specimens ("Na-polyP" coat and "Ca-polyP-MP" coat) were submersed in 24-well cell culture plates, under otherwise standard condition, with medium/serum, for a period of up to 3 d. Where indicated, cells were added at the beginning of the experiments at a concentration of 2×10^4 cells per 3 mL to the bone specimens.

For the light microscopic inspections, the cells were, after the termination of the experiments, stained with Calcein AM (#17783; Sigma) to visualize/analyze the cells.[63] Microscopy was performed with the Olympus-IX70-inverted/fluorescence microscope (Olympus, Hamburg; Germany).

EDX Analysis: The EDX experiments were performed with an EDAX Genesis EDX System that is attached to a scanning electron microscope

(Nova 600 Nanolab, FEI, Eindhoven; The Netherlands). The analyses were performed at 10 kV with a collection time of 30–45 s. Areas of 5–10 μm^2 were analyzed. In a first semiquantitative approximation, the signals corresponding to the respective elements were quantitated.[64]

XRD Analysis: XRD of dried powder samples was measured with a Philips PW 1820 diffractometer with monochromatic Cu-Kα radiation ($\lambda = 1.5418$ Å, 40 kV, 30 mA, 5 s, $\Delta\theta = 0.02$), as described.[9]

FTIR Spectroscopy: FTIR spectroscopy was performed with an ATR-FTIR spectroscope/Varian 660-IR spectrometer (Agilent, Santa Clara; CA), equipped with a Golden Gate ATR unit (Specac, Orpington; UK). Each spectrum was collected from an average of 100 scans with a spectral resolution of 4 cm^{-1} (typically 500–2000 cm^{-1}). The baseline corrections and analyses of the spectra were implemented with the Varian 660-IR software package 5.2.0 (Agilent). The graphical display was realized with Origin Pro (version 8.5.1; OriginLab, Northampton; MA). The spectral peaks were assigned according to published data.[9,58]

Determination of the Mechanical Properties: The mechanical properties were determined with a nanoindenter using the NanoTest Vantage System (Micro Materials Ltd, Wrexham; UK). This system was equipped with a Berkovich diamond indenter and allowed for a continuous depth-sensing nanoindentation.[65] 40 independent measurements were performed at one distinct site of the respective sample under the following conditions; temperature 25 °C, maximum depth limit 1 µm, loading/unloading speed 0.4 mN s^{-1}, and hold at the maximum load for 30 s. The spacing between two adjacent indents was at least 30 µm. The Martens hardness (HM) as well as the elastic modulus (E) was calculated according to the described procedure.[65] The following values for operating the indenter diamond were selected: Poisson ratio $\nu = 0.07$ and elastic modulus E = 1143 GPa.[66] For the measurement of bone material the Poisson ratio ν = 0.36 was used.[67] All calculations were performed with the Nano-Test Platform Four V.40.08 software package.

Cultivation/Mineralization of Cells: Human osteogenic sarcoma cells (SaOS-2 cells)[25] were purchased (Sigma #89050205). They were grown in McCoy's medium (containing 1×10^{-3} M $CaCl_2$) with 5% heat-inactivated fetal calf serum (FCS), 2×10^{-3} M L-glutamine and gentamicin (50 µg mL^{-1}) in six-well plates (Sigma-Greiner) as described.[68] The cells were seeded at a density of 2×10^4 cells per 3 mL well and cultivated for 3 d in medium/FCS. The cultures remained untreated (controls) or were treated for up to 8 d with 50 µg mL^{-1} of "Na-polyP" coat or "Ca-polyP-MP" coat. In the assays with polyP, the culture assays were enriched with 2×10^{-3} M $CaCl_2$ in order to avoid any depletion of Ca^{2+} ions required for hydroxyapatite deposition.[69]

For ESEM analysis glutaraldehyde fixated cells were processed through acetone dehydration steps and finally critical point dried, as described above.

MTT Viability Assay: To determine the growth rate of the cells, they were seeded into well plates and cultured for 1 or 3 d in medium/serum in the absence of polyP (controls) or with 50 µg mL^{-1} of "Na-polyP" coat or "Ca-polyP-MP" coat. Then the viability/cell growth was determined by the colorimetric MTT (# M2128, Sigma) assay.[70] In brief, the cells were incubated first with 1 µg mL^{-1} of MTT (2 h) and subsequently with 20% SDS in 50% dimethyl-formamide (Sigma; 24 h). The formazan grains were dissolved and the optical density was measured at 595 nm.

Mineralization by SaOS-2 Cells In Vitro: For the mineralization studies, SaOS-2 cells were incubated in culture medium/serum in the absence or presence of polyP (50 µg mL^{-1} of Na-polyP or Ca-polyP-MP) for 3 d. Then the cultures were supplemented with the mineralization activation cocktail (MAC), required for initiation of hydroxyapatite-like formation and incubation was continued for additional 3–8 d. This cocktail included the inducers 50×10^{-3} M ascorbic acid and 10×10^{-9} M dexamethasone.[68,71] Glycerophosphate was not included into the cocktail, because polyP could substitute, after hydrolysis with the ALP that is present in serum, for this organophosphate, as described.[43] Then the cultures were stained with 10% alizarin red S (staining for ossification), as described.[72] The intensity of alizarin red S staining was quantitatively assessed by application of a spectrophotometric assay.[73] The optical density was read at 405 nm. The amount of bound alizarin red S, given in moles, was determined from a calibration curve.[73] Finally the values were normalized to total DNA, which was assessed by using the PicoGreen method;[74] calf thymus DNA was used as a standard.

Statistical Analysis: After verification that the respective values follow a standard normal Gaussian distribution and that the variances of the respective groups are equal, the results were statistically assessed using the independent two-sample Student's t-test.[75]

Acknowledgements

The authors thank Ms. Kerstin Bahr, Institute of Functional and Clinical Anatomy, University Medical Center of the Johannes Gutenberg University, Mainz (Germany) for continuous support in cell culture and electron microscopy. Likewise, the authors thank Mr. G. Glaßer [Electron Microscopy], Max Planck Institute for Polymer Research, Mainz (Germany) for continuous support. W.E.G.M. is the holder of an ERC Advanced Investigator Grant (grant number 268476). In addition, W.E.G.M. obtained three ERC-PoC grants (Si-Bone-PoC, Grant No.: 324564; MorphoVES-PoC, Grant No.: 662486; and ArthroDUR, Grant No.: 767234). Finally, this work was supported by grants from the European Commission (grant numbers 604036 and 311848), the International Human Frontier Science Program and the BiomaTiCS research initiative of the University Medical Center, Mainz.

Conflict of Interest

The authors declare no conflict of interest.

Keywords

biologization, bone repair, human osteogenic sarcoma (SaOS-2) cells, Inorganic polyphosphate, nano/microparticles

Received: June 29, 2019
Revised: July 27, 2019
Published online: August 28, 2019

[1] R. Setiawati, P. Rahardjo, *Bone Development and Growth*, IntechOpen, https://www.intechopen.com/online-first/bone-development-and-growth, **2018**.
[2] J. R. Dwek, *Skeletal Radiol.* **2010**, *39*, 319.
[3] W. K. Ovalle, P. C. Nahirney, F. H. Netter, *Netter's Essential Histology*, Elsevier/Saunders, Philadelphia, PA, USA **2013**.
[4] S. Debnath, A. R. Yallowitz, J. McCormick, S. Lalani, T. Zhang, R. Xu, N. Li, Y. Liu, Y. S. Yang, M. Eiseman, J. H. Shim, M. Hameed, J. H. Healey, M. P. Bostrom, D. A. Landau, M. B. Greenblatt, *Nature* **2018**, *562*, 133.
[5] C. K. Chan, E. Y. Seo, J. Y. Chen, D. Lo, A. McArdle, R. Sinha, R. Tevlin, J. Seita, J. Vincent-Tompkins, T. Wearda, W. J. Lu, K. Senarath-Yapa, M. T. Chung, O. Marecic, M. Tran, K. S. Yan, R. Upton, G. G. Walmsley, A. S. Lee, D. Sahoo, C. J. Kuo, I. L. Weissman, M. T. Longaker, *Cell* **2015**, *160*, 285.
[6] L. Idolazzi, E. Ridolo, A. Fassio, D. Gatti, M. Montagni, M. Caminati, I. Martignago, C. Incorvaia, G. Senna, *Eur. J. Inter. Med.* **2017**, *38*, 12.
[7] J. H. Morrissey, S. H. Choi, S. A. Smith, *Blood* **2012**, *119*, 5972.
[8] H. C. Schröder, L. Kurz, W. E. G. Müller, B. Lorenz, *Biochemistry* **2000**, *65*, 296.
[9] W. E. G. Müller, E. Tolba, H. C. Schröder, S. Wang, G. Glaßer, R. Muñoz-Espí, T. Link, X. H. Wang, *Mater. Lett.* **2015**, *148*, 163.

[10] H. Masuki, T. Okudera, T. Watanebe, M. Suzuki, K. Nishiyama, H. Okudera, K. Nakata, K. Uematsu, C. Y. Su, T. Kawase, *Int. J. Implant Dent.* **2016**, *2*, 19.
[11] H. C. Blair, Q. C. Larrouture, Y. Li, H. Lin, D. Beer-Stoltz, L. Liu, R. S. Tuan, L. J. Robinson, P. H. Schlesinger, D. J. Nelson, *Tissue Eng., Part B* **2017**, *23*, 268.
[12] F. N. Syed-Picard, G. A. Shah, B. J. Costello, C. Sfeir, *J. Oral Maxillofac. Surg.* **2014**, *72*, 1078.
[13] A. L. Boskey, *BoneKEy Rep.* **2013**, *2*, 447.
[14] Y. Iwasaki, J. J. Kazama, H. Yamato, M. Fukagawa, *Bone* **2011**, *48*, 1260.
[15] O. O. Aruwajoye, H. K. Kim, P. B. Aswath, *Calcif. Tissue Int.* **2015**, *96*, 324.
[16] W. E. G. Müller, M. Neufurth, J. Huang, K. Wang, Q. Feng, H. C. Schröder, B. Diehl-Seifert, R. Muñoz-Espí, X. H. Wang, *ChemBioChem* **2015**, *16*, 1323.
[17] E. Tolba, W. E. G. Müller, B. M. A. El-Hady, M. Neufurth, F. Wurm, S. Wang, H. C. Schröder, X. H. Wang, *J. Mater. Chem. B* **2016**, *4*, 376.
[18] W. E. G. Müller, H. C. Schröder, U. Schlossmacher, V. A. Grebenjuk, H. Ushijima, X. H. Wang, *Biomaterials* **2013**, *34*, 8671.
[19] X. H. Wang, M. Ackermann, S. Wang, E. Tolba, M. Neufurth, Q. Feng, H. C. Schröder, W. E. G. Müller, *Biomed. Mater.* **2016**, *11*, 035005.
[20] X. H. Wang, S. Wang, F. He, E. Tolba, H. C. Schröder, B. Diehl-Seifert, W. E. G. Müller, *Adv. Eng. Mater.* **2016**, *18*, 1406.
[21] N. Mikolajewicz, E. A. Zimmermann, B. M. Willie, S. V. Komarova, *eLife* **2018**, *16*, 7.
[22] Q. Yao, C. Yu, X. Zhang, K. Zhang, J. Guo, L. Song, *Bone* **2017**, *97*, 175.
[23] W. E. G. Müller, E. Tolba, Q. Feng, H. C. Schröder, J. S. Markl, M. Kokkinopoulou, X. H. Wang, *J. Cell Sci.* **2015**, *128*, 2202.
[24] W. E. G. Müller, E. Tolba, H. C. Schröder, X. H. Wang, *Macromol. Biosci.* **2015**, *15*, 1182.
[25] J. Fogh, J. M. Fogh, T. Orfeo, *J. Natl. Cancer Inst.* **1977**, *59*, 221.
[26] S. B. Rodan, Y. Imai, M. A. Thiede, G. Wesolowski, D. Thompson, Z. Bar-Shavit, S. Shull, K. Mann, G. A. Rodan, *Cancer Res.* **1987**, *47*, 4961.
[27] C. Pautke, M. Schieker, T. Tischer, A. Kolk, P. Neth, W. Mutschler, S. Milz, *Anticancer Res.* **2004**, *24*, 3743.
[28] E. Tolba, X. H. Wang, M. Ackermann, M. Neufurth, R. Muñoz-Espí, H. C. Schröder, W. E. G. Müller, *Adv. Sci.* **2018**, *2018*, 1801452.
[29] E. Loughrill, D. Wray, T. Christides, N. Zand, *Matern. Child Nutr.* **2017**, *13*, e12368.
[30] W. E. G. Müller, S. Wang, E. Tolba, M. Neufurth, M. Ackermann, R. Muñoz-Espí, I. Lieberwirth, G. Glasser, H. C. Schröder, X. H. Wang, *Small* **2018**, *14*, 1801170.
[31] F. Rauch, *J. Musculoskeletal Neuronal Interact.* **2005**, *5*, 194.
[32] N. Li, J. Song, G. Zhu, X. Li, L. Liu, X. Shi, Y. Wang, *Biomater. Sci.* **2016**, *4*, 1554.
[33] S. Matsushima, N. Isogai, R. Jacquet, E. Lowder, T. Tokui, W. J. Landis, *Cells Tissues Organs* **2011**, *194*, 320.
[34] O. Duchamp de Lageneste, A. Julien, R. Abou-Khalil, G. Frangi, C. Carvalho, N. Cagnard, C. Cordier, S. J. Conway, C. Colnot, *Nat. Commun.* **2018**, *9*, 773.
[35] A. Graja, F. Garcia-Carrizo, A. M. Jank, S. Gohlke, T. H. Ambrosi, W. Jonas, S. Ussar, M. Kern, A. Schürmann, K. Aleksandrova, M. Blüher, T. J. Schulz, *Aging Cell* **2018**, *17*, e12810.
[36] B. J. Quirk, K. Sannagowdara, E. V. Buchmann, E. S. Jensen, D. C. Gregg, H. A. T. Whelan, *J. Clin. Orthop. Trauma* **2016**, *7*, 234.
[37] J. H. Park, B. W. Park, Y. H. Kang, S. H. Byun, S. C. H. Wang, D. R. Kim, D. K. Woo, J. H. Byun, *Cell Biochem. Funct.* **2017**, *35*, 497.
[38] W. C. Lee, A. R. Guntur, F. Long, C. J. Rosen, *Endocr. Rev.* **2017**, *38*, 255.
[39] A. Sakkas, F. Wilde, M. Heufelder, K. Winter, A. Schramm, *Int. J. Implant Dent.* **2017**, *3*, 23.
[40] D. J. Lee, S. Diachina, Y. T. Lee, L. Zhao, R. Zou, N. Tang, H. Han, X. Chen, C. C. Ko, *J. Tissue Eng.* **2016**, *7*, 204173141668030.
[41] M. D. Hoffman, D. S. Benoit, *Clin. Orthop. Relat. Res.* **2013**, *471*, 721.
[42] X. H. Wang, H. C. Schröder, W. E. G. Müller, *J. Mater. Chem. B* **2018**, *6*, 2385.
[43] W. E. G. Müller, X. H. Wang, B. Diehl-Seifert, K. Kropf, U. Schloßmacher, I. Lieberwirth, G. Glasser, M. Wiens, H. C. Schröder, *Acta Biomater.* **2011**, *7*, 2661.
[44] B. Lorenz, H. C. Schröder, *Biochim. Biophys. Acta, Protein Struct. Mol. Enzymol.* **2001**, *1547*, 254.
[45] H. Orimo, *J. Nippon Med. Sch.* **2010**, *77*, 4.
[46] W. E. G. Müller, M. Ackermann, E. Tolba, M. Neufurth, I. Ivetac, M. Kokkinopoulou, H. C. Schröder, X. H. Wang, *Biochem. J.* **2018**, *475*, 3255.
[47] W. E. G. Müller, S. Wang, M. Neufurth, M. Kokkinopoulou, Q. Feng, H. C. Schröder, X. H. Wang, *J. Cell Sci.* **2017**, *130*, 2747.
[48] W. E. G. Müller, M. Ackermann, S. F. Wang, M. Neufurth, R. Muñoz-Espí, Q. L. Feng, H. C. Schröder, X. H. Wang, *Cell. Mol. Life Sci.* **2018**, *75*, 21.
[49] J. Jeong, J. H. Kim, J. H. Shim, N. S. Hwang, C. Y Heo, *Biomater. Res.* **2019**, *23*, 4.
[50] E. I. F. Pearce, *Calcif. Tissue Int.* **1981**, *33*, 395.
[51] S. L. Rowles, in *Structural and Chemical Organization of Teeth* (Ed: A. E. W. Miles), Academic Press, New York, USA **1967**, pp. 201–240.
[52] N. Kourkoumelis, I. Balatsoukas, M. Tzaphlidou, *J. Biol. Phys.* **2012**, *38*, 279.
[53] L. C. Palmer, C. J. Newcomb, S. R. Kaltz, E. D. Spoerke, S. I. Stupp, *Chem. Rev.* **2008**, *108*, 4754.
[54] M. Vallet-Regí, D. A. Navarrete, in *Nanoceramics in Clinical Use: From Materials to Applications*, 2nd ed., Nanoscience & Nanotechnology (Eds: M. Vallet-Regí, D. A. Navarrete), Royal Society of Chemistry, London, England **2016**, pp. 1–29.
[55] W. R. Stoll, W. F. Neuman, *J. Am. Chem. Soc.* **1956**, *78*, 1585.
[56] G. Boivin, *Medicographia* **2007**, *29*, 126.
[57] W. F. Neuman, M. W. Neuman, *Chem. Rev.* **1953**, *53*, 1.
[58] G. Nagy, T. Lorand, Z. Patonai, G. Montsko, I. Bajnoczky, A. Marcsik, L. Mark, *Forensic Sci. Int.* **2008**, *175*, 55.
[59] E. A. Cavalcanti-Adam, T. Volberg, A. Micoulet, H. Kessler, B. Geiger, J. P. Spatz, *Biophys. J.* **2007**, *92*, 2964.
[60] A. Giacomini, M. Ackermann, M. Belleri, D. Coltrini, B. Nico, D. Ribatti, M. A. Konerding, M. Presta, M. Righi, *Angiogenesis* **2015**, *18*, 499.
[61] B. Bharat, in *Modern Tribology Handbook*, Vol. *2* (Ed: B. Bharat), Taylor & Francis/CRC Press, Milton Park-Didcot, UK **2000**, Ch. 2, pp. 1–72.
[62] D. Bray, in *Supercritical Fluid Methods and Protocols, Methods in Biotechnology (MIBT)*, Vol. *13* (Eds: J. R. Williams, A. A. Clifford), Humana Press, New York, USA **2000**, pp. 235–243.
[63] W. E. G. Müller, S. F. Wang, M. Ackermann, M. Neufurth, R. Steffen, E. Mecja, R. Muñoz-Espí, Q. L. Feng, H. C. Schröder, X. H. Wang, *Int. J. Mol. Sci.* **2017**, *18*, 2154.
[64] M. Scimeca, S. Bischetti, H. K. Lamsira, R. Bonfiglio, E. Bonanno, *Eur. J. Histochem.* **2018**, *62*, 2841.
[65] W. C. Oliver, G. M. Pharr, *J. Mater. Res.* **1992**, *7*, 1564.
[66] J. M. Williams, A. Adewunmi, R. M. Schek, C. L. Flanagan, P. H. Krebsbach, S. E. Feinberg, S. J. Hollister, S. Das, *Biomaterials* **2005**, *26*, 4817.
[67] F. Katsamanis, D. D. Raftopoulos, *J. Biomech.* **1990**, *23*, 1173.
[68] M. Wiens, X. H. Wang, U. Schloßmacher, I. Lieberwirth, G. Glasser, H. Ushijima, H. C. Schröder, W. E. G. Müller, *Calcif. Tissue Int.* **2010**, *87*, 513.
[69] G. Williams, J. D. Sallis, *Calcif. Tissue Int.* **1982**, *34*, 169.
[70] M. B. Hansen, S. E. Nielsen, K. Berg, *J. Immunol. Methods* **1989**, *119*, 203.
[71] F. Langenbach, J. Handschel, *Stem Cell Res. Ther.* **2013**, *4*, 117.
[72] A. Young, D. E. Phipps, A. B. Astroff, *Teratology* **2000**, *61*, 273.
[73] C. A. Gregory, W. G. Gunn, A. Peister, D. J. Prockop, *Anal. Biochem.* **2004**, *329*, 77.
[74] H. C. Schröder, A. Borejko, A. Krasko, A. Reiber, H. Schwertner, W. E. G. Müller, *J. Biomed. Mater. Res., Part B* **2005**, *75B*, 387.
[75] A. Petrie, P. Watson, *Statistics for Veterinary and Animal Science*, Wiley-Blackwell, Oxford, England **2013**, pp. 85–99.